JOURNAL OF Materials CHEMISTRY

A low resistance boron-doped carbon nanotube–polystyrene composite

Paul C. P. Watts,[a] Wen Kuang Hsu,[a] George Z. Chen,[b] Derek J. Fray,[b] Harold W. Kroto[a] and David R. M. Walton[a]

[a]*School of Chemistry, Physics and Environmental Science, University of Sussex, Brighton, UK BN1 9QJ*
[b]*Department of Materials Science and Metallurgy, University of Cambridge, Pembroke Street, Cambridge, UK CB2 3QZ*

Received 3rd April 2001, Accepted 20th June 2001
First published as an Advance Article on the web 20th August 2001

A composite made from boron-doped carbon nanotubes and polystyrene exhibits relatively low electrical resistance and minor variations in conduction when mechanically loaded. Carbon nanotubes form a network within the plastic film, thereby establishing electrical conduction uniformly throughout the composite. Individual carbon nanotubes behave as intrinsic resistors, therefore the film resistance obeys Ohm's law.

Introduction

The resistivity of carbon-based conducting polymers usually lies in the 10^{6}–10^{-2} Ω m range, *e.g.* higher than the values commonly found for doped polyacetylene (10^{-3} Ω m) and bulk graphite (10^{-4}–10^{-5} Ω m).[1] Accordingly, carbon-based polymers have limited uses as anti-static components. Another drawback is that carbon–polymer composites commonly exhibit localized conduction, due to the uneven distribution of carbon particles. This phenomenon becomes significant when conducting films are subject to mechanical loading (*e.g.* compression and bending). Film bending causes simultaneous segregation and aggregation of carbon particles, resulting in variable conduction. The conducting path within composite films depends upon internal crystallite dimensions and the degree of aggregation of spherical particles;[2] the greater the crystallite size, the lower the resistance. Increase in the carbon content of polymers results in: (a) a change in the intrinsic properties of the polymer (*e.g.* T_g); (b) an increase in particle contact resistance, and (c) minimization of localized conduction: factors (b) and (c) compete. However, economic routes to conducting polymers with low carbon content and low resistance, coupled with minor variations in conductivity under mechanical loading, are required for useful applications (*e.g.* lithium–polymer batteries). Conductivity measurements, either on individual or bulk carbon nanotubes (CNs), have been studied widely.[3–10] Recently, the impedance of bulk CVD-made CNs has been measured and the CNs have been found to exhibit characteristics of an *RLC* circuit (*i.e.* resistance–inductance–capacitance).[11] This result is inconsistent with a previous report which claimed that individual arc-made CNs behave as intrinsic resistors.[12] This inconsistency may arise from the presence of other carbon materials (*e.g.* flake-like and amorphous carbon) and metal particles.[11] Accordingly, interfacial charging between different materials (*i.e.* carbon and metals) occurs, generating a capacitor-like structure. Meanwhile, the circular/spiral current passing through interwoven nanotubes in the CVD-made CNs possibly results in an inductor-like electronic response.[3,11]

The electronic behaviour of CNs in the polymer matrices has so far attracted limited attention.[13,14] In this paper, we have studied the AC impedance of CNs in a polystyrene matrix. In order to investigate the nature of carbon-based conducting polymers, we have introduced various materials, *e.g.* fullerene-free carbon soot (FFCS), pyrolysed-polyacetylene carbon black (PPCB), graphite powder (GP), multi-walled carbon nanotubes (MWCNs) and boron-containing multi-walled carbon nanotubes (BMWCNs), into the polystyrene. The BMWCN-film (12.5% by weight) exhibited a relatively low resistivity (3.2 Ω m) and the conduction did not vary significantly upon mechanical compression and bending.

Experimental

The FFCS, MWCNs and BMWCNs were produced by the carbon arc process, as described previously.[15] The MWCNs and BMWCNs were subject to micro-filtering and mild oxidation in order to remove polyhedral particles and the amorphous carbon coating from CN surfaces.[16,17] However, TEM revealed that carbon particles were still present, albeit in relatively low concentrations, compared with unoxidized materials. GP and PPCB were purchased from Fluka-Chemie (Switzerland) and PTS (UK) respectively. Polymer composites were produced by mixing the appropriate carbon material with a solution of polystyrene (2 g, Aldrich, UK) in toluene (20–30 cm^3) in various ratios (*i.e.* 2.5, 5, 7.5, 10 and 12.5%, carbon-to-polymer, by weight). The carbon-containing polymer solutions were ultra-sonicated (10 min), then transferred to a Petri dish (9 × 1.3 cm) and the dish was subjected to a vacuum (10^{-2} Torr) in order to remove the toluene. The resulting GP, FFCS, MWCN and BMWCN-films (*ca.* 0.3 mm thick) were easily detached from the dish using a scalpel. The PPCB-film was very fragile, and only small fragments (*ca.* 1–3 cm^2) were obtained. Accordingly, a hot-compact carbon black-based conducting polystyrene (HCCBCP, 1 mm thick, unknown carbon black ratio, Goodfellow, UK) was examined instead, together with a BMWCN-film of the same dimensions (1 mm thick, 12.5%) for comparative purposes. In order to study the distribution of carbon in the polymer, the films were ground and dispersed in water for TEM investigations. Owing to the elongated nanotube structure, the differences in morphology between the MWCNs (or BMWCNs) and the polymer can be easily distinguished. However, the image contrast of the polymer matrix does not differ from that of other carbon materials (*i.e.* FFCS, GP and PPCB) either in back-scattering (SEM) or dark-field image mode (TEM). Therefore, the distribution of FFCS, GP and PPCB in the

 DOI: 10.1039/b102989b

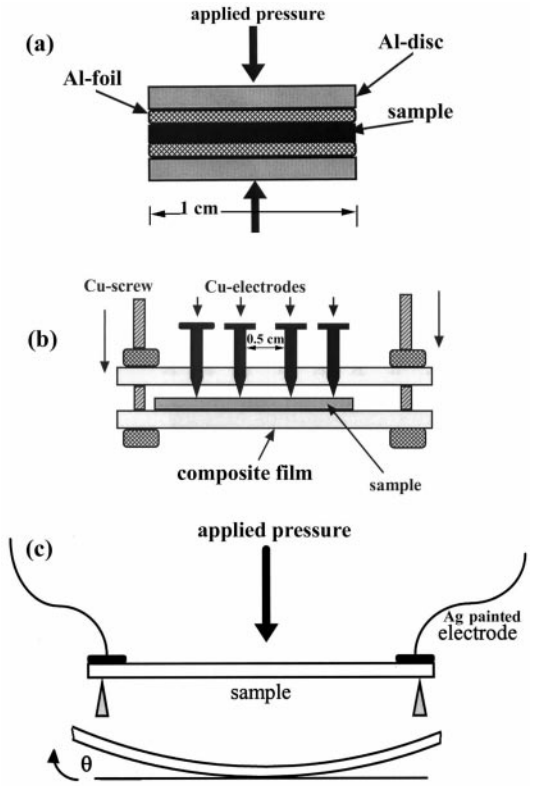

Fig. 1 (a) Device for two-probe measurement. (b) Device for four-probe measurement. (c) Design for film bending test.

polymer matrix remains unclear. For AC impedance measurements (Solartron 1260 Frequency Response Analyzer) at room temperature, two- and four-probe geometries were employed. The composite films and electrodes were assembled so that the film was sandwiched between two Al-discs (1 cm diameter) suitable for a two-probe test (Fig. 1a). A *ca.* 20 kg load was then applied to the discs. For the four-probe test, the film was sandwiched between two fibre-plastic plates (Tufnol, RS, UK), one of which contained four aligned needle-like Cu screws (*ca.* 0.5 cm apart). The plates were tightened and the Cu-electrodes were screwed down so as to maximize contact with the film (Fig. 1b). For two- or four-probe tests, the samples were examined under loading (*vide supra*). The film bending test was carried out using silver wire electrodes (3 cm apart), attached by means of silver paint to the films (1×5 cm), so that each film could be bent manually and reversibly during multiple meter monitoring (Fig. 1c). The bending angle lay in the 0–45° range.

Results and discussion

1. Distribution of carbon particles in the polystyrene matrix

Impedance measurements were carried out successfully on two samples, *i.e.* MWCN- and BMWCN-composite films (12.5%), for the following reasons: (a) the FFCS-film did not conduct for all sample ratios; (b) conduction occurred only on one face of the GP-film for all ratios; (c) the PPCB-film fragments exhibited localized conduction for all ratios; *i.e.* the resistance is greater on one face of the film than on the other (the difference is one or two orders of magnitude, as indicated by a multiple meter). Here we define the top and bottom faces of the film as those faces exposed to the vacuum and in contact with the Petri dish respectively. The bottom face of the film always exhibited a lower electrical resistance compared with the top (*e.g.* for GP-film and PPCB fragments). The MWCN-film also displayed localized conduction when the MWCN content of the polymer was less than 12.5%. The localized conduction disappeared at 10% for BMWCN-films, *i.e.* when the resistance on the top and bottom faces of the film was of the same order of magnitude. The presence of one conducting face only (*i.e.* GP-film) or a difference in resistance between the top and bottom faces (*e.g.* PPCB-fragments, or low content MWCNs and BMWCNs in the polymer) is indicative of a gradient distribution of the carbon component throughout the matrix. The fact that the resistance of the bottom face is less implies the presence of denser aggregated carbon, possibly due to particle settlement during film formation (Fig. 2a). In order to verify this contention, the polymer solution containing 12.5% MWCNs or BMWCNs was transferred to a larger Petri dish (11.3×1.3 cm) so as to form a thinner (0.2 mm) film, *i.e.* reducing the particle precipitating effect (Fig. 2b). The outcome supports our contention. First, the films exhibit resistances of the same order of magnitude on both faces at lower ratios, 7.5% for MWCN and 5% for BMWCN-films respectively. Second, the resistance of both faces increases for MWCN and BMWCN-films, as compared with the 0.3 mm films. The increase in resistance, when the film is thinner and wider (*i.e.* maintaining the same overall volume), is due to a decrease in carbon density per unit area. Third, the GP-film maintains the one-face conduction phenomenon, but the resistance increases.

2. TEM and SEM analyses

Fig. 3 illustrates the structure of carbon materials before incorporation into the polymer: (a) FFCS, (b) PPCB, (c) GP and (d) MWCNs (4–10 μm in length). The BMWCN and MWCN structures are essentially identical (*i.e.* 5–40 nm diameter), except that the former is longer ($\geqslant$20 μm) and contains *ca.* 1–5% boron incorporated into the hexagonal network.[15,17] In Fig. 3, several features are distinguishable: (a) the FFCS exhibits an interconnected particle-like morphology (insert); (b) the internal structure of the FFCS is amorphous, no clear crystalline fringes being present; (c) the morphology of bulk PPCB is similar to that of FFCS; (d) the PPCB particles are hollow and the wall structures are relatively well-graphitized (insert: L_c 2–4 nm, L_a 5–10 nm), as compared with FFCS; (e) the PPCB particles are interconnected *via* the carbon walls; (f) the GP consists of large segregated carbon fragments (300–500 nm); (g) the MWCNs and BMWCNs are aggregated without preferential tube alignments. The large GP fragments undergo significant settlement during film formation, which explains why one-face conduction is always present in GP-film.

Fig. 4a shows an SEM image of a BMWCN-film (cross-section 0.3 mm). The film thickness is fairly uniform and its

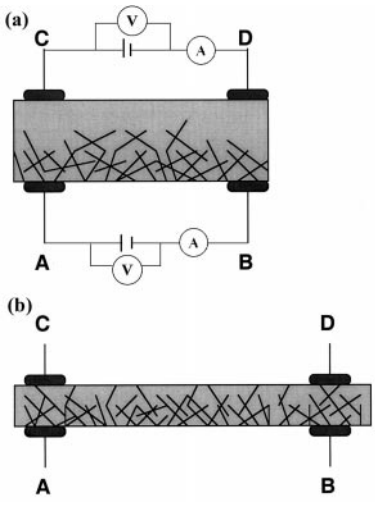

Fig. 2 (a) Carbon distribution in the thicker film. Conduction occurs only at the bottom face (A–B connection), not at the top face (C–D connection). (b) Carbon distribution in thin film. Conduction occurs at the top (C–D connection) and bottom faces (A–B connection).

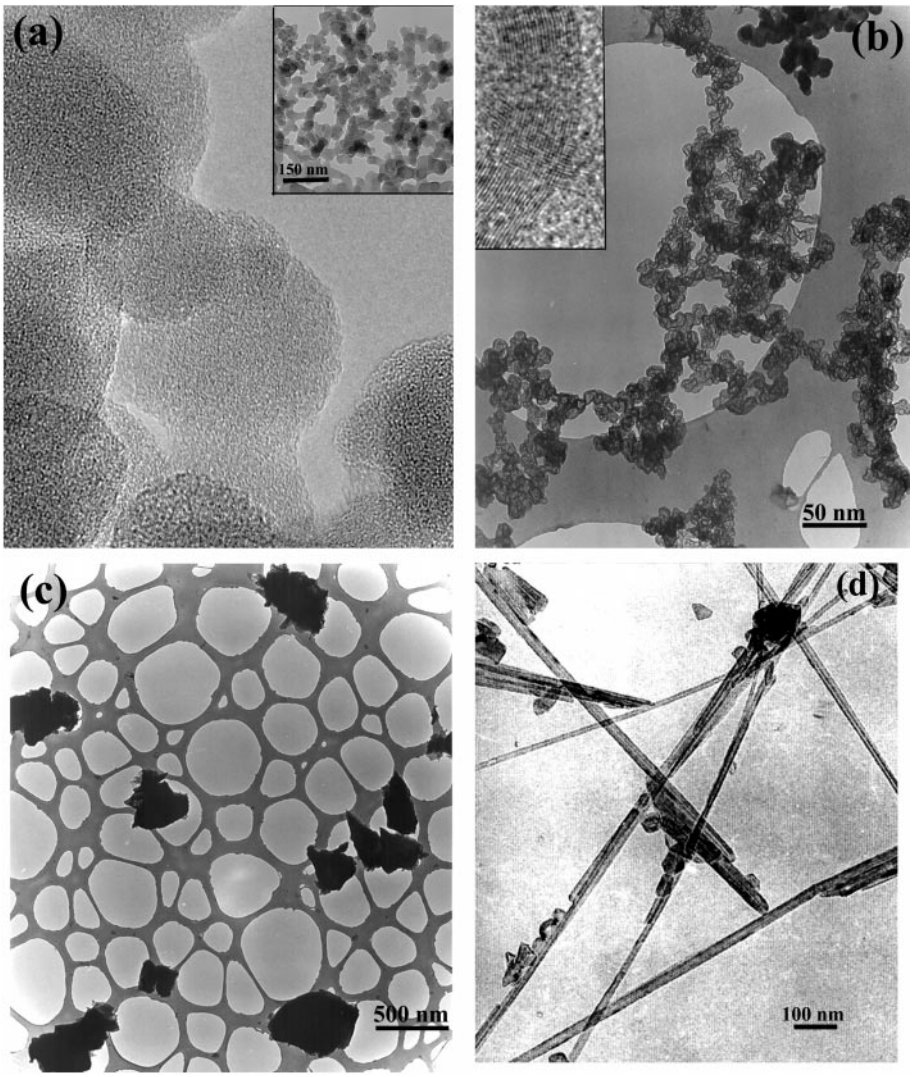

Fig. 3 TEM images of (a) FFCS, (b) PPCB, (c) GP and (d) MWCNs. Insert (a): Morphology of bulk FFCS. Insert (b): HRTEM image of PPCB.

internal structure consists of small dark voids, surrounded by a white composite matrix (Fig. 4b). Fig. 5 shows typical SEM and TEM images of BMWCNs in the polymer. The tubes are arranged randomly within the matrix (Fig. 5a). Tube–tube contact, either *via* tube bundling or tube–tube crossing, is evident (*e.g.* Fig. 5b), and the electrical conducting path is therefore established. TEM also reveals the presence of polymer-coated nanotubes (arrows, Fig. 5c). The coating influences the tube–tube contact structure. First, if the individual tube surface coatings are established after tube–tube contact, the tube–tube contact structure will be strongly maintained. Second, if the nanotubes are coated before tube–tube contact, the coating prevents electrical contact between adjacent tubes.

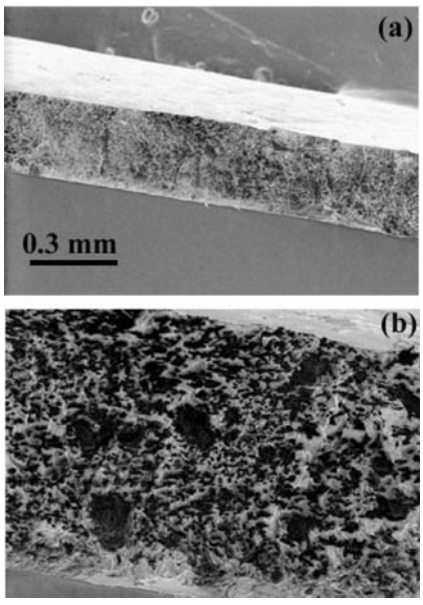

Fig. 4 (a) SEM images of BMWCN-film cross section (0.3 mm thick). (b) Enlarged SEM image from (a).

Various electrical contacts exist in the polymer matrix, including tube–tube, tube–particle and particle–particle. However, the tube–tube contact dominates, because the quantity of particle present is limited by oxidation. The resistivity along the *c*-axis is *ca.* 3–4 orders of magnitude greater than along the in-plane direction (10^{-6}–10^{-7} Ω m) in graphite,[5] due to the difficulty in electron flow across the 3.4 Å layer separation. Nanotubes in contact (*i.e.* basal plane in contact) implies that the electrons flow within the polymer matrix *via* routes of lowest resistance.

Fig. 6 shows the surface morphologies of BMWCN-films (0.3 mm thick), top and bottom faces respectively, for various concentrations. Based on Fig. 6, a few features were distinguishable along with the electrical resistance recording. (a) At low concentrations (*i.e.* 2.5–5%), the difference in resistance between the top and bottom faces is *ca.* one order of magnitude, which is also reflected in the different morphologies

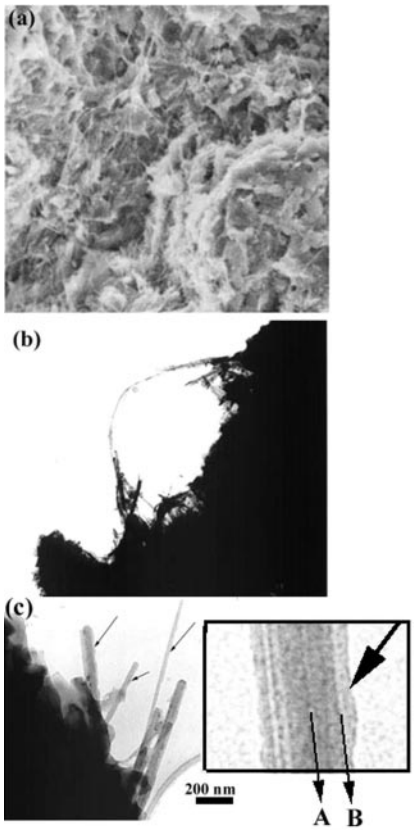

Fig. 5 (a) SEM image of BMWCNs in polystyrene. (b) TEM image of BMWCNs in polystyrene. (c) TEM image of polymer coated MWCNs (arrows). Insert: enlarged TEM image of coated MWCN. Large arrow: polymer coating. Arrow A: central core of carbon nanotube. Arrow B: the carbon nanotube surface. The fringe contrast is darker in the coated carbon nanotube body than in the coating polymer.

seen in Figs. 6a and c (top faces) and Figs. 6b and d (bottom faces). In Figs. 6a and c, the surface morphology consists of white islands, surrounded by dark regions. The largest island is *ca.* 0.5–1.2 μm wide. The bottom face morphology (Figs. 6b and d) is similar to sand-paper surfaces. We did not observe nanotubes protruding from the top and bottom faces, in fact the nanotubes are likely to be embedded in the polymer with either tube bodies or tube tips partly exposed to air. The formation of sand-paper surface-like structures (bottom face) possibly reflects the presence of denser nanotube aggregates. The white and dark regions seen in the top faces (Figs. 6a and c) are either tube-rich or tube-poor, however we were unable to locate tube-rich regions by SEM. The surface morphology of both top and bottom faces is essentially the same when the BMWCN concentration exceeds 7.5% (Fig. 6e–h). In other words, nanotubes are evenly spread throughout the polystyrene matrix. The 1 mm thick BMWCN-film exhibits a similar phenomenon when present to the extent of 7.5%.

3. Impedance measurements

a. Compression. Fig. 7a–c shows two-probe impedance spectra of MWCN and BMWCN-films (0.3 mm thick) under 20 kg loading, together with 1 mm thick BMWCNs and HCCBCP-films. The HCCBCP impedance varies within the 10^3–10^5 Ω range for all frequencies (100–10 000 Hz) (Fig. 7a). Variation begins at *ca.* 12 000 Ω (10 000 Hz, arrow 3, Fig. 7c), and gradually increases to 38 300 Ω at 260 Hz (arrow 4, Fig. 7c). The impedance value eventually reaches 36 600 Ω (arrow 5, Fig. 7c). Nanotube-based composite films exhibit relatively low impedances ($2–5 \times 10^2$ Ω) without significant variation in conduction (Figs. 7a and b). The BMWCN-films, either 0.3 mm (175 Ω) or 1 mm (450 Ω) thick, exhibit an impedance one order of magnitude lower (Fig. 7b) compared to MWCNs (3000 Ω). Small humps are distinguishable in the MWCN-films (arrows 1 and 2, Fig. 7c). Unfortunately, four-point impedance measurements could not be carried out on the thin MWCN and BMWCN-films (0.3 mm thick), due to film penetration by the Cu needle electrodes. Fig. 7d shows the results of four-probe measurements on the 1 mm thick BMWCN and HCCBCP films. The impedance of the HCCBCP-film varies drastically, in marked contrast to the BMWCN-film (700 Ω, corresponding to 3.2 Ω m resistivity).

b. Bending. The variation of the HCCBCP resistance becomes significant when the film is bent, the amplitude being one to two orders of magnitude. The variation in BMWCN resistance lies within the 10–30 Ω range when the film is bent.

The electron microscope and impedance measurements give rise to several points:

1. Two factors contribute to the electrical resistance of composite films: (a) internal crystallinity of the carbon particles and (b) the establishment of electrical contact between carbon particles. The lack of structural regularity in these particles renders current flow difficult. The insulation exhibited by the FFCS-film in our study is mainly due to factor (a) because the FFCS is amorphous; no crystal domains are present to allow current flow.

2. Network formation, *via* tube–tube bundling and crossing within the polymer matrix, results in relatively low resistance at low carbon-to-polymer ratios (10–12.5%), as compared with spherical carbon particle-based conducting polymers (50%, carbon-to-polymer commonly found in industry). This conducting network is robust and is less segregated than the spherical carbon particles when loaded. We assume that the pressure applied (20 kg) to the composite film induces small polymer creep during impedance tests.[18,19] The spherical carbon particles segregate and aggregate simultaneously in the presence of creep, resulting in conductivity variation (HCCBCP-film, Fig. 7a and d). Tube–tube detachment or separation is difficult. For example, the surface coating (insert, Fig. 5c), maintains tube–tube contact to some extent in the presence of loading. A possible explanation is illustrated in Fig. 8a, which shows two coating-free crossed nanotubes. If polymer creep propagates at the crossing point, tubes separate (route 1, Fig. 8a). Tube sliding, one over the other, occurs if the creep proceeds in the direction vertical to the tube axis (route 2, Fig. 8a). Tube–tube contact can then be maintained by surface coating, resulting in slightly inward bending of the tube (route 1, Fig. 8b) or outward bending (route 2, Fig. 8b). According to previous reports,[18,19] tube bending in the polymer has been observed (Fig. 5b) and prevails when the polymer matrix is loaded. Meanwhile, when the tube–polymer composite is compressed, the load transferred from the matrix to the tubes results only in outer shell tube stress.[19] In other words, the tube–tube is able to maintain contact with minor-distorted outer shells.

3. The drastic variation in the HCCBCP impedance profile (Figs. 7c and d) mainly arises from the presence of a capacitor component. (a) According to Fig. 3b, carbon black consists of graphitic domains within the particle walls, which lower the electrical resistance.[2] In other words, the electrical resistance in the particle will be much lower than the particle–particle contact resistance (*ca.* two/three orders of magnitude difference). Consequently, a capacitor-like structure is produced, *i.e.* metal/insulator/metal (particle/contact resistance/particle). The presence of the capacitor component will influence the impedance profile. According to the following equation, the impedance $Z=[R^2+(X_L-X_C)^2]^{1/2}$, R: resistance, X_L: inductive reactance, X_C: capacitive reactance. If the composite film contains capacitor and inductor components, *i.e.* $X_L \neq 0$, $X_C \neq 0$, then the impedance profile is non-linear. (b) Carbon

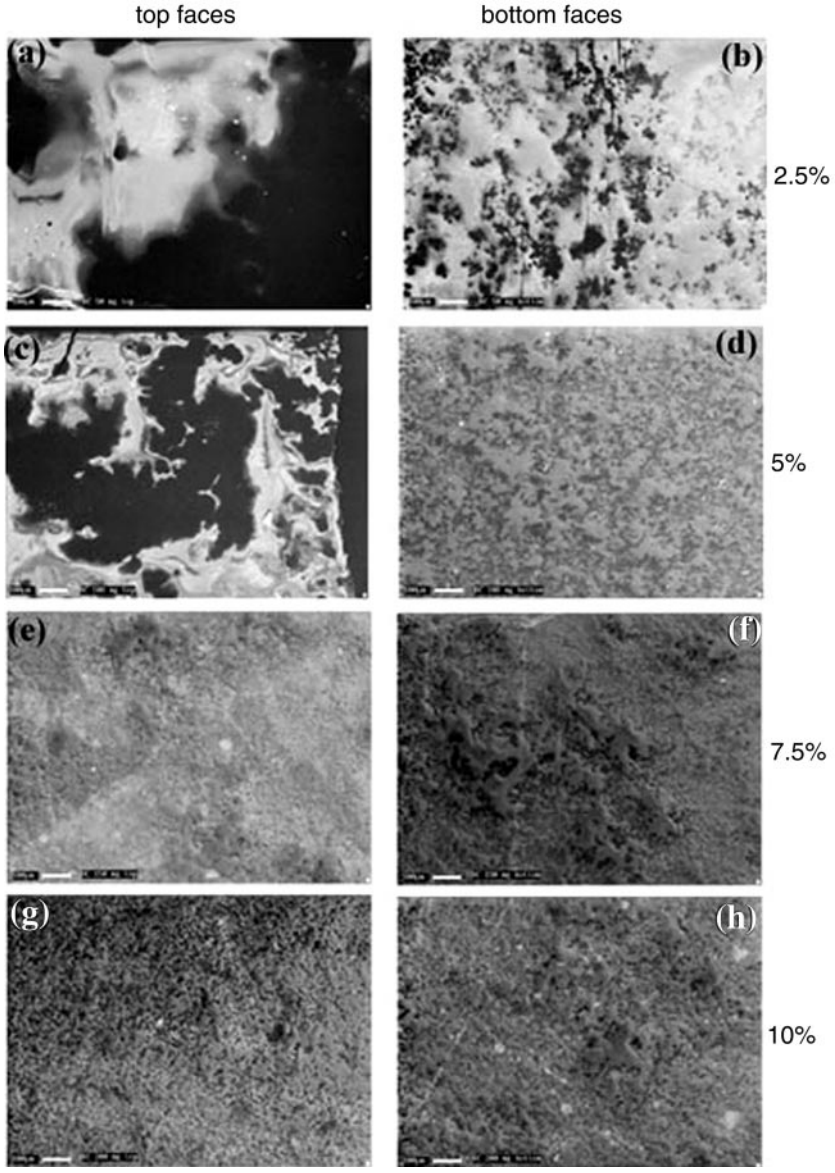

Fig. 6 SEM images of top and bottom face morphologies with various BMWCN contents: (a–b) 2.5%; (c–d) 5%; (e–f) 7.5% and (g–h) 10%.

black usually contains heteroatoms (*e.g.* H, O and S), which form metallic or insulating islands within the particles, or in the carbon lattice. If metallic islands (*e.g.* odd-alternate π-type radicals)[20] are formed, the charge carriers travel *via* tunneling from one metallic island to another.[21] Accordingly, the capacitor-like structure (metallic island/contact resistance/metallic island) is also generated within aggregated particles. For the MWCN- and BMWCN-films, the presence of a linear and horizontal impedance profile is indicative of the intrinsic resistors, *i.e.* $X_L = X_C = 0$, and $Z = R$.

The geometry of two- and four-probe measurements may also give rise to variation in the impedance profile, due to contact resistance between film and electrodes. In the two-probe test, the film surfaces were entirely covered by an Al disc, which minimizes the contact resistance. In the case of four-probe tests, four aligned Cu needle electrodes were brought into contact with the film. If the distribution of the carbon component around the Cu electrodes is not uniform, the contact resistance increases. This contention is supported by the presence of less variation in two-probe impedance profiles than in the four-probe system (HCCBCP-film, Figs. 7a, d). However, the BMWCN-film exhibits linear and horizontal impedance profiles, either in a two- or four-probe test, implying the presence of uniform tube distribution in the polymer.

4. The lower impedance in the BMWCN-film compared to the MWCN-film arises because boron-doping of carbon nanotubes results in increases in charge density on CNs.[17,22] The BMWCNs exhibit lower resistivity, in bulk and in polymer, indicating that electrical conduction within the polymer is actually established *via* individual tube–tube contact, not *via* electron hopping from tube to tube. As described above, nanotubes are intrinsic resistors, therefore the conducting network in the matrix can be expressed as a combination of resistors in parallel ($1/R_{eff} = 1/R_1 + 1/R_2 \ldots$, *i.e.* tube bundling) and in series ($R_{eff} = R_1 + R_2 \ldots$, *i.e.* tube–tube crossing); R_1, $R_2 \ldots$ represent individual nanotube resistors. If electron hopping from tube to tube is present as a major conduction mechanism, then the intrinsic resistance of the tube (*i.e.* R_n, $n = 1, 2 \ldots$) will not significantly contribute to the R_{eff} value, either in parallel or in series. In other words, the R_{eff} value of the BMWCN-film will not differ significantly from that of the MWCN-film, as long as the carbon contents of both composites are identical. In practice, the R_{eff} value of the BMWCN-film is one order of magnitude smaller than the R_{eff} value of the MWCN-film, indicating that individual tubes contribute to the overall R_{eff}.

5. The BMWCNs are much longer than MWCNs. The longer tubes lead to preferential networking and percolation in the polymer at relatively low concentrations.[14]

6. The presence of a small variation in the MWCN-film

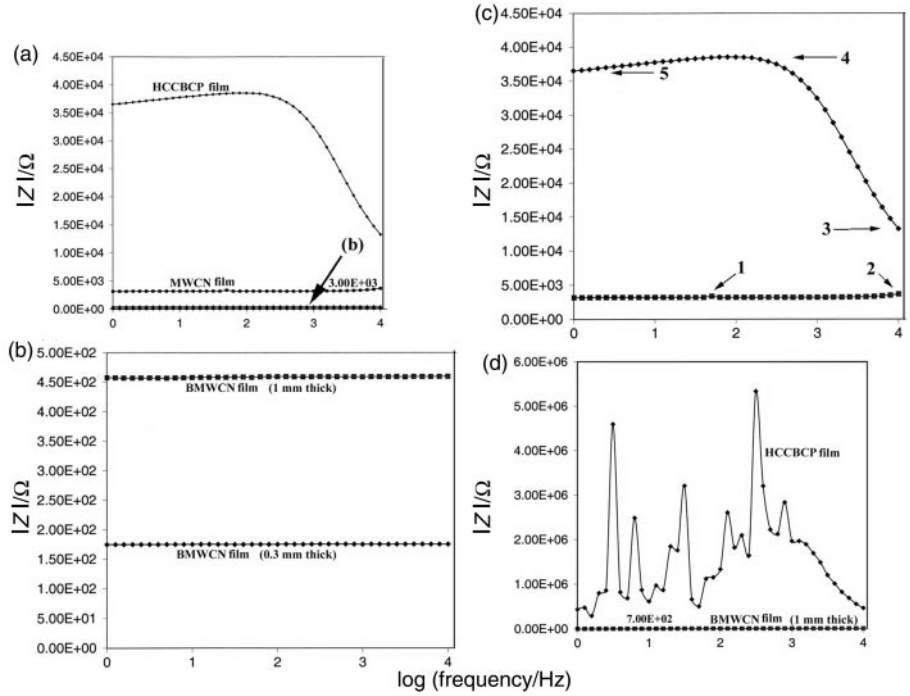

Fig. 7 (a) Two-probe impedance spectra of carbon materials as labeled. $|Z|$: the impedance modulus. (b) Enlarged impedance spectra of two BMWCN-films from (a). (c) Enlarged impedance spectra of HCCBCP and MWCN-films from (a). (d) Four-probe impedance spectra of HCCBCP and BMWCN-films (both 1 mm thick).

(arrows, Fig. 7c) possibly arises as follows. The bulk MWCNs contain both semiconducting and metallic tubes.[23] The former exhibit a 0.1–1 eV band gap. The MWCN tube–tube contact in the polymer is established *via* combination of (a) metallic–semiconducting tubes, (b) metallic–metallic tubes and (c) semiconducting–semiconducting tubes. When the current flows between (b) and (c), a capacitor-like structure is produced.

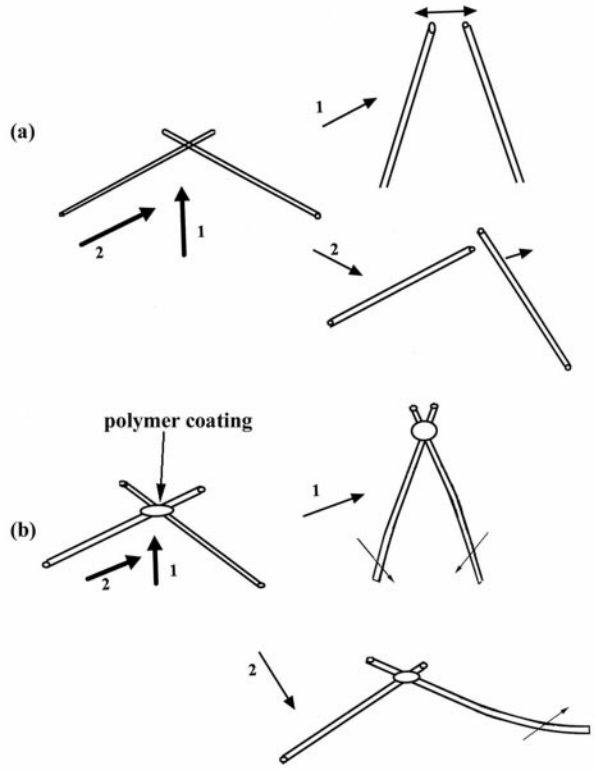

Fig. 8 (a) Possible separation process for uncoated tubes. (b) Possible bending process for coated tubes.

Summary

(1). The conducting composite, carbon nanotubes–polystyrene, exhibits relatively low resistance at low carbon-to-polymer ratios.

(2). The method for producing a nanotube–polymer composite is straightforward and can be applied to other polymer matrices.

(3). The conducting network within the tube–polymer composite is constructed by combining tube–tube crossing and bundling. Such a network exhibits linear and horizontal impedance profiles when compressed.

(4). The conducting nanotube–polystyrene composite is essentially an ohmic conductor at frequencies $1–10^4$ Hz.

(5). The relatively low resistance of BMWCN-films is due to the intrinsic low resistance of boron-doped nanotubes and to preferential networking.

(6). The composites made from polystyrene and particle-like carbon structures (*e.g.* graphite powder, carbon black and arc-generated soot) exhibit high resistance and localised conduction. The electrical conduction in particular varies significantly when the film is mechanically loaded.

(7). The capacitor- and inductor-like behaviour was not observed when the arc-made carbon nanotubes were used as electrical conducting components within the plastic matrix.

Acknowledgements

We thank the Leverhulme Trust, the Royal Society and the EPSRC (UK) for financial support, and J. Thorpe and D. Randall (Sussex) for assistance with the electron microscopy.

References

1 A. R. Blythe, *Polym. Testing*, 1984, **4**, 195.
2 X. Bourrat, *Carbon*, 1993, **31**, 287.
3 H. G. Dai, E. W. Wong and C. M. Lieber, *Science*, 1996, **272**, 523.
4 D. L. Carroll, Ph. Redlich, X. Blase, J.-C. Charlier, S. Curran, P. M. Ajayan, S. Roth and M. Rühle, *Phys. Rev. Lett.*, 1998, **81**, 2332.

5 B. Q. Wei, R. Spolenak, Ph.K. Redlich, M. Rühle and E. Arzt, *Appl. Phys. Lett.*, 1999, **74**, 3149.
6 T. W. Ebbesen, H. J. Lezec, H. Hiura, J. W. Bennett, H. F. Ghaemi and T. Thio, *Nature*, 1996, **382**, 54.
7 M. Baxendale, K. G. Lim and G. A. Amaratunga, *Phys. Rev. B*, 2000, **61**, 12705.
8 W. A. de. Heer, W. S. Bacsa, A. Châtelain, T. Gerfin, R. H. Baker, L. Forró and D. Ugarte, *Science*, 1995, **268**, 845.
9 G. Baumgartner, M. Carrard, L. Zuppiroli, W. Bacsa, W. A. de. Heer and L. Forró, *Phys. Rev. B*, 1997, **55**, 6704.
10 R. Seshadri, H. N. Aiyer, A. Govindaraj and C. N. R. Rao, *Solid State Commun.*, 1994, **91**, 195.
11 N. A. Prokudina, E. R. Shishchenko, O. S. Joo, D. Y. Kim and S. H. Han, *Adv. Mater.*, 2000, **12**, 1444.
12 S. Frank. Ph. Poncharal, Z. L. Wang and W. A. de. Heer, *Science*, 1998, **280**, 1744.
13 Ph. G. Colins and A. Zettl, *Appl. Phys. Lett.*, 1996, **69**, 1969.
14 G. Z. Chen, M. S. P. Shaffer, D. Coleby, G. Dixon, W. Zhou, D. J. Fray and A. H. Windle, *Adv. Mater.*, 2000, **12**, 522.
15 O. Stephan, P. M. Ajayan, C. Colliex, Ph. Redlich, J. M. Lambert, P. Bernier and P. Lefin, *Science*, 1994, **266**, 1683.
16 T. W. Ebbesen, P. M. Ajayan, H. Hiura and K. Tanigaki, *Nature*, 1994, **367**, 519.
17 W. K. Hsu, S. Firth, Ph. Redlich, M. Terrones, H. Terrones, Y. Q. Zhu, N. Grobert, H. W. Kroto and D. R. M. Walton, *J. Mater. Chem.*, 2000, **10**, 1425.
18 O. Lourie, D. M. Cox and H. D. Wagner, *Phys. Rev. Lett.*, 1998, **81**, 1638.
19 L. S. Schadler, S. C. Giannaris and P. M. Ajayan, *Appl. Phys. Lett.*, 1998, **73**, 3842.
20 L. J. Dunne, A. K. Sarkar, H. W. Kroto, J. Munn, P. Kathirgamanathan, U. Heinen, J. Fernandez, J. P. Hare, D. G. Reid and A. D. Clark, *J. Phys. Condens. Matter*, 1996, **8**, 2127.
21 L. J. Dunne, A. D. Clark, M. F. Chaplin and H. Katbamna, *Carbon*, 1992, **30**, 1227.
22 W. K. Hsu *et al.*, *Chem. Phys. Lett.*, 2000, **323**, 572.
23 J. W. Mintmire, B. I. Dunlap and C. T. White, *Phys. Rev. Lett.*, 1992, **68**, 520.